



The Triple Phase Boundary

A Mathematical Model and Experimental Investigations for Fuel Cells

Ryan O'Hayre,^{a,z} David M. Barnett,^b and Fritz B. Prinz^c

^aDepartment of Materials Science and Engineering, Rapid Prototyping Laboratory,

^bDepartment of Materials Science and Engineering and Department of Mechanical Engineering,

^cDepartment of Mechanical Engineering and Department of Materials Science and Engineering, Stanford University, Stanford, California 94305-3030, USA

A mathematical model is developed which describes the nature, properties, and scaling of the triple phase boundary (TPB) for a Pt/Nafion polymer electrolyte membrane fuel cell (PEMFC) system. The model incorporates coupled reaction and diffusion phenomena, leading to a concept of the TPB not as a singularity, but rather as having an "effective width." The "effective width" of the TPB depends on the interplay between the relative rates of the reaction and diffusion processes at the Pt/Nafion interface. Implications of the model for PEMFC catalyst layer design are explored. Additionally, scaling predictions of the model are compared with kinetic observations from geometrically well-defined Pt-microelectrode/Nafion experiments and are shown to match favorably with experimental results.

© 2005 The Electrochemical Society. [DOI: 10.1149/1.1851054] All rights reserved.

Manuscript submitted May 25, 2004; revised manuscript received July 21, 2004. Available electronically January 12, 2005.

The idea of the triple phase boundary (TPB) is extensively employed in the fuel cell literature, especially with respect to solid oxide fuel cells (SOFCs) and polymer electrolyte membrane fuel cells (PEMFCs). The TPB concept holds that the hydrogen oxidation reaction (HOR) and the oxygen reduction reaction (ORR) can only occur at confined spatial sites, called "triple phase boundaries" where electrolyte, gas, and electrically connected catalyst regions contact. A simplified schematic of the TPB is shown in Fig. 1. The reaction kinetics (especially the ORR kinetics) often present a significant limitation to fuel cell performance. Therefore, understanding, characterizing, and optimizing the TPB content in fuel cells provides excellent opportunities for performance enhancement.

On the technology side, efforts to increase the amount of TPB in technological fuel cells by using nanostructured catalyst layers have proven highly successful. By employing nanoscale composites of catalyst material, conductive support, solid electrolyte, and gas pore space, investigators have been able to dramatically increase the amount of TPB, thus improving kinetic performance.^{1,2}

From a scientific perspective, recent efforts have been made to more clearly delineate the nature and properties of the TPB. In many of these studies, there is a growing realization that the simple concept of the TPB as a singularity is unrealistic; rather, it should be thought of as a "zone," whose width, properties, and behavior depend on a complex interplay between coupled reaction and diffusion processes. Most of this work has focused on SOFCs.³⁻⁸ In contrast, few studies have considered PEMFC systems.^{9,10} One exception is the work by Iczkowski and Cutlip,¹⁰ who treated reaction and diffusion in an acidic liquid electrolyte-based fuel cell using an agglomerate model of the catalyst layer. Their work produces an "effectiveness factor" which depends on the relative rates of reaction and diffusion in the catalyst layer. However, the agglomerate treatment of the catalyst layer makes it difficult to correlate this effectiveness factor to the catalyst geometry or TPB structure.

In this paper we develop a mathematical model which seeks to clearly describe the nature, properties, and scaling of the TPB for a Pt/Nafion PEMFC system. As a general framework, the model is applicable to both SOFC and PEMFC systems; minor changes are required for application to SOFCs. Implications of the model for PEMFC catalyst layer design are explored. Additionally, scaling predictions of the model are compared to kinetic observations from geometrically well-defined Pt-microelectrode/Nafion experiments and are shown to match favorably with experimental results.

TPB Model

The nature of the TPB is determined by the combination of the reaction processes that occur at the catalyst/electrolyte interface and by the diffusion processes which supply reactants to this interface. These coupled processes are visually illustrated in Fig. 2, which describes the basic geometry of our TPB model. The electrode phase in the model represents a catalytically active material. In the case of a PEMFC system, for example, this electrode may represent a catalytically active platinum particle (of $2a$ width), which is in simultaneous contact with Nafion electrolyte and the gas phase. While realistic catalyst structures are a chaotic, random mixture of electrolyte, gas pores, catalyst particles, and conductive support powders, we restrict ourselves to the simplified geometry shown in Fig. 2 in order to achieve a workable analytic model.

We furthermore make several additional simplifying assumptions, including:

1. The gas-phase reactant concentration is constant. (Gas-phase mass transport is neglected.)
2. The reactant concentrations across the gas/electrolyte interface are in equilibrium. (Incorporation is fast compared to diffusion through the electrolyte.)
3. Transport (diffusion) of reactants through the electrode is neglected.
4. Only the bulk diffusion path is considered (no surface diffusion).
5. Reaction is limited to the electrode/electrolyte interface.
6. Oxygen is the rate-determining species for the ORR. (Proton supply is not limiting.)
7. We restrict ourselves to two-dimensional steady-state diffusion, *i.e.*, $\partial^2 c / \partial x^2 + \partial^2 c / \partial y^2 = 0$, where $c(x, y)$ is the concentration.

Using symmetry and neglecting electrode diffusion, a mathematical quarter-space proves sufficient to frame the model, as illustrated in Fig. 3. At steady state, the rates of diffusion (reactant supply) and reaction (reactant consumption) at the electrode/electrolyte interface exactly balance. We have explicitly assumed that the reaction rate is first order with respect to the reactant. Experimental observations of the ORR appear to confirm this assumption.^{11,12} The other boundary conditions are set by the symmetry of the system and the reactant gas initial concentration. These boundary conditions are summarized: (i) along the y -axis ($x = 0$): $\partial c / \partial x = 0$ (due to symmetry); (ii) along the x -axis ($y = 0$) for ($0 \leq x < a$): $-D \partial c / \partial y + kc = 0$; and (iii) along the x -axis ($y = 0$) for ($a \leq x < \infty$): $c = c_0$. Here, c (mol/cm³) is the concentration of the rate-determining reactant species (*i.e.*, O₂ for the case of the ORR), c_0 (mol/cm³) is the initial concentration of the reactant in the

^z E-mail: rohayre@stanford.edu

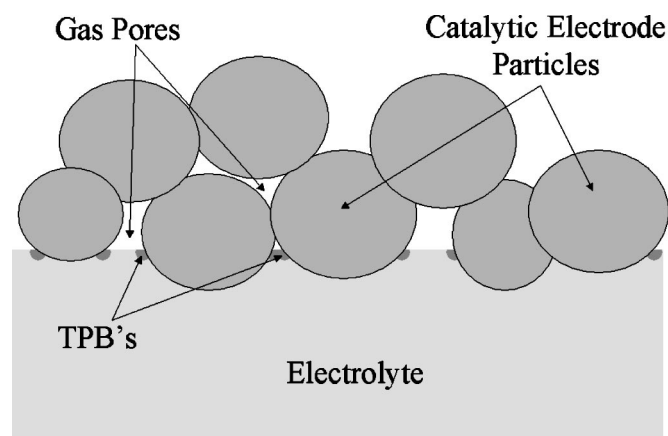


Figure 1. A simplified schematic diagram of the electrode/electrolyte interface in a fuel cell, illustrating the TPB reaction zones where the catalytically active electrode particles, electrolyte phase, and gas pores intersect.

electrolyte (this is set by the Henry's law solubility of the reactant in the electrolyte), $2a$ (cm) is the size of the catalyst electrode particle, D (cm²/s) is the diffusion coefficient, and k (cm/s) is the heterogeneous reaction rate constant at the electrode/electrolyte interface.

Due to the mixed boundary conditions imposed on this model, the solution is facilitated by employment of the conformal mapping technique.¹³ The mathematical details of this method of solution are outlined in Appendix A. In the next section, the key results of the model are discussed.

TPB Model Results

We are interested in the model results at the electrolyte/electrode interface ($Y = y/a = 0$). Solution of the model at $Y = 0$ gives the following general form for the concentration profile as a function of distance along the $X = x/a$ axis (underneath the catalyst electrode particle)

$$c(X, 0) = c_0 \left\{ 1 - \frac{4ha}{\pi} \sum_{n=0}^{\infty} (-1)^n \frac{\cos[(2n+1)\sin^{-1}X]}{(2n+1)(2n+1+ha)} \right\}; \quad 0 \leq X \leq 1 \quad [1]$$

where $h = k/D$. Essentially, h is a lumped kinetic term that incorporates the relative balance between the rates of reaction and diffusion in the system. The quantity ha is a dimensionless length which relates the kinetic scale of the problem ($1/h$) to the real scale of the system (a), and because ha appears in both the numerator and de-

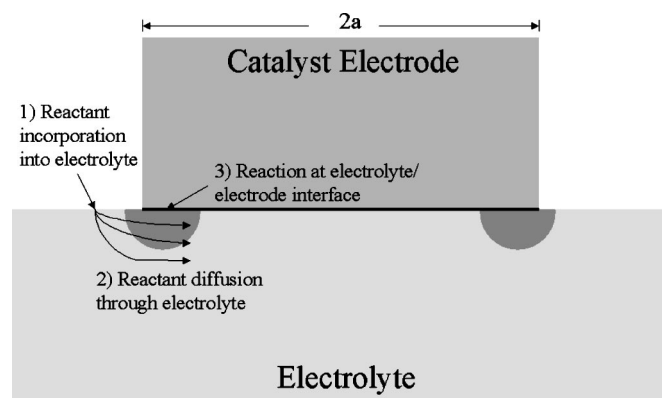


Figure 2. Physical processes governing the nature and properties of the TPB.

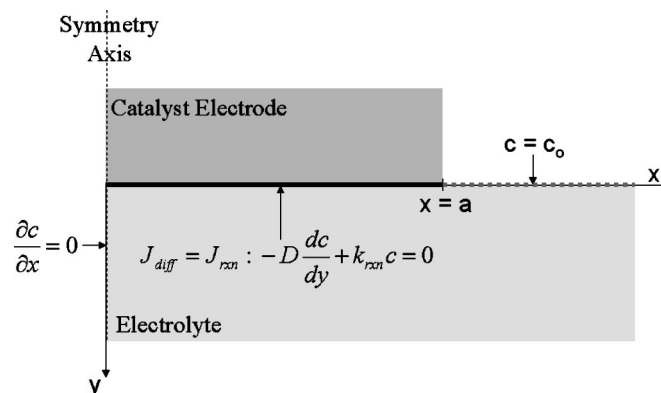


Figure 3. Quarter space model of the TPB.

ominator of the infinite sum, the relative magnitude of ha determines the form of the solution. For large enough n , the series in Eq. 1 converges as $(-1)^n ha / (2n+1)^2$. Further details on the convergence of the solution for large and small ha are given in Appendix A.

Figure 4 plots dimensionless concentration profiles derived from Eq. 1 for various values of ha . These profiles were obtained using the first 75 terms in the infinite series. As ha increases, the number of terms necessary to achieve a satisfactory solution increases rapidly, as visibly demonstrated by the oscillations apparent in the $ha = 20$ curve. Note that these profiles do not show self-similarity; for example, the solution for $ha = 1$ does not superimpose on the first 10% of the solution for $ha = 10$. Self-similarity is destroyed due to the existence of two characteristic length scales ($1/h$ and a) in this problem.

From an inspection of the profiles, it is apparent that the reactant concentration under the catalyst electrode begins to show significant depletion for $ha > 1$. An "effective TPB width" may be associated with the shape of these concentration profiles. There are many ways to define the TPB width, including a decay width (representing the length scale at which the reactant concentration has dropped to $1/e$ of its original value), or an integral width (representing the length scale at which, say, $2/3$ of the current density from the reaction has occurred). However, for the sake of simplicity and generality, we choose to define the TPB width as the length scale where $ha = 1$

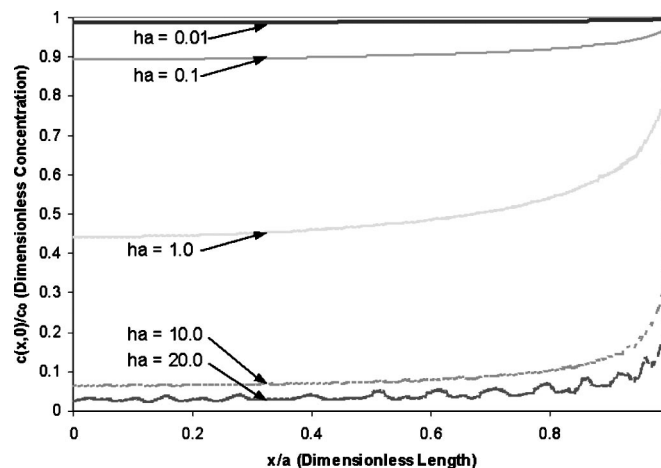


Figure 4. Dimensionless concentration profiles ($c(x, 0)/c_0$) vs. dimensionless length (x/a) for various values of ha . Profiles are derived from the TPB model following Eq. 1.

Table I. Calculated ORR TPB width values from the TPB model for various ORR overpotentials. Calculations based on D_{O_2} , $c_0(O_2)$, and kinetic reaction parameters listed in the text, following Eq. 6.

ORR overpotential (mV)	w_{TPB} (nm)
400	7.93×10^5
600	1.71×10^4
800	368
1000	7.93
1200	0.171

$$w_{TPB} = \frac{1}{h} \quad [2]$$

Here w_{TPB} (nm) is the effective TPB width. A benefit of this definition is that w_{TPB} depends only on the kinetic parameters embedded in h

$$w_{TPB} = \frac{D}{k} \quad [3]$$

As the reaction rate (k) at the electrode/electrolyte interface increases, w_{TPB} decreases. In contrast, if the diffusion rate (D) increases, w_{TPB} increases. For electrochemical systems, the heterogeneous reaction rate constant, k , may be expressed in terms of the current density of the electrochemical reaction, j_{rxn}

$$k = \frac{j_{rxn}}{c_0} \quad [4]$$

The reaction current density, j_{rxn} (A/cm²), may be estimated from the Tafel equation¹⁴ for a given overpotential, η

$$j_{rxn} = j_0 10^{\eta/b} \quad [5]$$

where j_0 is the exchange current density (A/cm²), η is the overpotential (mV), and b is the Tafel slope (mV).

Combining Eq. 3-5 allows us to express the TPB width in terms of well-known or easily measurable quantities

$$w_{TPB} = \frac{Dc_0}{j_0 10^{\eta/b}} \quad [6]$$

We are especially interested in the TPB properties associated with the ORR, because the kinetics of the ORR account for the majority of the activation losses in PEMFCs. Parthasarathy *et al.*¹⁵ have measured both the diffusion coefficient and the solubility of O₂ gas in Nafion under standard conditions; $D_{O_2} = 7.4 \times 10^{-7}$ cm²/s, $c_0(O_2) = 5.98 \times 10^{-6}$ mol/cm³ (after adjustment by Henry's law for $p_{O_2} = 0.21$ atm). We use their numbers in the calculations that follow; others researchers have reported similar values for D_{O_2} and $c_0(O_2)$ in Nafion.^{11,16-18}

Typical Tafel kinetic parameters for the ORR for platinum/Nafion systems at standard conditions are $j_0 \approx 10^{-8}$ A/cm² and $b \approx 120$ mV.^{11,15,16,18-22} Combining these parameters from the literature with Eq. 6 allows the calculation of effective TPB widths for various values of the ORR overpotential; Table I summarizes these results. As can be seen from the table, the effective TPB width is strongly dependent on the ORR overpotential. At high reaction rates (high overpotential) the reaction is restricted to a very narrow region in the direct vicinity of the TPB. At low reaction rates (low overpotential) the reaction extends diffusely across the electrode/electrolyte interface.

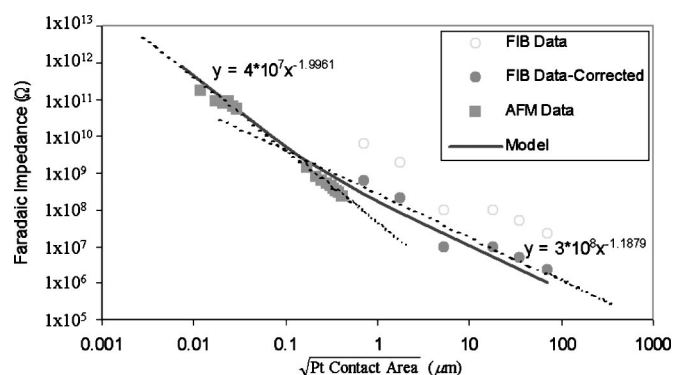


Figure 5. Faradaic impedance (R_f) vs. Pt/Nafion contact size for (○) FIB-patterned Pt/Nafion microelectrode⁹ experiments and (■) Pt/Nafion AFM point contact²³ experiments. (●) Corrected FIB-patterned Pt/Nafion microelectrode data as described in the text. (---) Power law fits to the data denoting a change in slope from ~ -1 to ~ -2 , indicating a transition from perimeter-based scaling to area-based scaling. This transition is predicted by the TPB model (—).

It is interesting to take a look at the effects of relaxing some of the assumptions we made during the formulation of this model. For example, if the first-order reaction limitation is relaxed to allow for higher order concentration dependence, the problem becomes nonlinear. The techniques used in Appendix A to solve the linear problem may still be applied to the nonlinear problem, but the unknown coefficients A_n (see Appendix A) must be obtained by solving an infinite set of nonlinear algebraic equations; this presents no real difficulty, as the system of equations may be truncated with confidence due to the nicely convergent nature of the series involved. As another example, introduction of surface diffusion at the Pt/Nafion interface proves difficult to incorporate mathematically. Qualitatively, however, the effect is simple to discuss; a fast surface diffusion term should extend the “effective width” of the TPB.

The full model solution given in Appendix A (Eq. A-7) allows for the calculation of the complete two-dimensional concentration profile underneath a catalyst particle. Mapping the solution back to the (x,y) plane allows for the concentration dependence in the y direction to be calculated. It is not difficult to deduce that the y -direction concentration profile shows a general power-law decay dependence with increasing depth (y).

TPB Model Implications and Experimental Comparisons

As mentioned previously, the parameter ha is a dimensionless length which relates the kinetic scale of the problem ($1/h$) to the real scale of the system (a). Further consideration of this parameter can provide insight for the design of catalyst structures. For example, when the real scale of a catalyst particle is less than the kinetic scale of the system, in other words, $a < 1/h$, then the whole catalyst/electrolyte interface is active for the electrochemical reaction. In contrast, if the real scale of a catalyst particle is much larger than the kinetic scale of the system ($a > 1/h$), then most of the reaction is limited to the perimeter of the particle. This observation suggests that appropriate length scales for the catalyst layer structure should be on the order of the size of the TPB width. In other words, optimal catalyst layer designs should ensure that most catalyst/electrolyte contacts are smaller than the extent of the TPB, so as to maximize kinetic effectiveness.

This scaling observation is corroborated by experimental findings from Pt-microelectrode/Nafion investigations. Measurements from well-defined Pt/Nafion microelectrodes⁹ and Pt/Nafion atomic force microscopy (AFM) point contacts²³ have produced the faradaic impedance (R_f) vs. Pt/Nafion contact size data shown in Fig. 5. Two features are immediately apparent in this data. First, it appears that the R_f values for the Pt-microelectrodes are offset to higher

impedance levels as compared with the AFM-tip data. In other words, the Pt microelectrodes kinetically perform much worse than the Pt AFM-tip/Nafion contacts. In fact, the Pt microelectrodes were prepared by direct focused ion beam (FIB) fabrication, and thus the platinum content in these electrodes was low. An energy-dispersive X-ray (EDX) study of the FIB deposited platinum has shown it to be approximately 30 atom % Pt, 70 atom % C. The closed circle data points and dashed-line trendline show the result if the R_f values for the Pt microelectrodes are simplistically adjusted to account for the dilutive effect of the carbon. A more important feature of the data is revealed by the power law fits to the two sets of experiments, which show a change in slope from -1.19 to -1.996 . Roughly, this slope change indicates a transition from perimeter-based scaling for the microelectrode experiments to area-based scaling for the nanoscale AFM contact measurements.

We believe that this transition in kinetic behavior represents the point at which the physical scale of the Pt/Nafion contact reaches the scale of the TPB width for this system. In other words, for Pt/Nafion contacts which are smaller than w_{TPB} , the entire interfacial area participates in the reaction because oxygen gas diffusion through the membrane is fast compared with reaction, but for contacts larger than w_{TPB} , the center becomes a “dead-zone” because the rate of oxygen gas diffusion is too slow.

This result can be recovered by our TPB model, as shown by the solid line in Fig. 5. (Details on the fitting parameters used for the model are provided in Appendix B.) The model correctly predicts the area-related kinetics (slope of ~ -2) for small contact sizes and the perimeter-related kinetics (slope of ~ -1) for large contact sizes. Additionally, the model correctly predicts the transition, or breakpoint, which occurs at a contact size between 100 nm and 1 μm .

Because the two sets of data were acquired in separate experiments, it should be acknowledged that fundamental differences in character between the two experiments could also account for the apparent change in kinetic behavior. For example, one concern is that the quality of the Pt/Nafion interface between the two sets of experiments could be very different. If the FIB-deposited Pt microelectrodes resulted in very “air-tight” Pt/Nafion interfaces (restricting oxygen access to the perimeter), while the contacts in the AFM-tip/Nafion experiments were “air-leaky” (providing ample oxygen access to the entire interfacial area), this could also explain the observed kinetic response.

Unfortunately, it is experimentally difficult to construct a single experiment which is able to span the entire length scale (from 10 nm to 100 μm) in order to more persuasively document the kinetic transition. Larger contact-area AFM tests are restricted by the lack of commercially available AFM cantilever probes of sufficient stiffness. Smaller-area FIB Pt-microelectrode experiments are currently prevented by the inability to define finer microelectrodes. We are currently considering the adoption of a nanoindentation instrument which may allow us to span the necessary length scales in a single experiment.

Conclusions

A simple mathematical model of the TPB for Pt/Nafion PEMFC systems has been developed which provides predicted concentration profiles underneath Pt/Nafion contacts. The model incorporates coupled reaction and diffusion phenomena, leading to a concept of the TPB not as a singularity, but having an “effective width.” The “effective width” of the TPB depends on the interplay between the relative rates of the reaction and diffusion processes at the Pt/Nafion interface; this is embedded in the kinetic term, $h = k/D$.

The simple analytical model of the TPB developed in this paper required several limiting assumptions. Numerical techniques (such as finite element) can avoid these simplifying assumptions, but often sacrifice the clarity and insight provided by an analytic solution. As discussed in the Results section, some of the model assumptions may be relaxed. Such modifications perhaps provides greater real-

ism, but at the expense of a more complex solution. This is an area for ongoing research and refinement.

The TPB model results suggest guidelines for effective PEM catalyst layer design. Appropriate length scales for the catalyst layer structure should be on the order of the size of the TPB width or smaller, so as to maximize kinetic effectiveness. Many potential catalyst layer configurations can be envisioned. Traditional PEM catalyst layers use mixtures of carbon-supported Pt particles, but spherical particle agglomerations present difficulties for controlling Pt/Nafion contact dimensions. Furthermore, spherical particles present inefficient surface-to-volume ratios. Geometries incorporating catalyzed nanowire “brushes” or planar multilayer catalyst structures consisting of alternating layers of Nafion and sputtered Pt catalyst may provide the ability to tune the catalyst layer periodicity to the TPB width, while also increasing surface-to-volume ratios and providing efficient current collection.

Most PEM fuel cells are carefully designed so that the catalyst layer is somewhat hydrophilic, while the diffusion backing and flow channels are hydrophobic. The hydrophobic diffusion layer and flow channels help to quickly remove water from the cell, reducing flooding problems. The catalyst layer itself is somewhat hydrophilic because it has been observed that a degree of water retention in the catalyst helps maximize kinetic performance. Thin water films may extend the amount of TPB in the catalyst layer by acting, like Nafion, as a transport layer for protons, thus activating the Pt particles that it coats. However, if the water layer is too thick, O_2 gas access is blocked. If the transport properties for O_2 and protons in water are similar to Nafion, then our TPB model might also be used to describe the optimal content, or coating of water inside the catalyst layer.

Acknowledgments

The authors warmly thank the members of the Rapid Prototyping Laboratory and especially the fuel cell team for their support. In particular, we recognize Dr. William D. Nix, Minhwan Lee, Dr. Turgut Gur, and Dr. Suk-Won Cha for their helpful insights and assistance with the study. This work was supported under a Stanford Graduate Fellowship. The Stanford Global Climate Energy Project (GCEP) provided funding for this research.

Stanford University assisted in meeting the publication costs of this article.

Appendix A

The steady-state diffusion boundary value problem discussed in the TPB model section of the text may be recast in “reduced form” by defining

$$\Omega(X, Y) = c(X, Y) - c_0 \quad [\text{A-1}]$$

where

$$\frac{\partial^2 c}{\partial x^2} + \frac{\partial^2 c}{\partial y^2} = 0; \quad X, Y \geq 0 \quad [\text{A-2}]$$

X and Y represent the dimensionless coordinates x/a and y/a , respectively, “ a ” is the half-width of the electrode, h and c_0 are constants, and the associated boundary conditions on Ω in the quarter space ($X, Y \geq 0$) are depicted in Fig. 6.

This mixed boundary value problem for Laplace’s equation (Eq. A-2) readily lends itself to solution by conformal mapping (see, for example, Churchill¹³). Consider the mapping

$$w = u + iv = \sin^{-1} z = -i \ln[iz + \sqrt{1 - z^2}] \quad [\text{A-3}]$$

where $z = X + iY$. The inverse mapping is

$$z = \sin w = \sin u \cosh v + i \cos u \sinh v \quad [\text{A-4}]$$

or

$$X = \sin u \cosh v; \quad Y = \cos u \sinh v \quad [\text{A-5}]$$

It is easily verified that the conformal mapping given by Eq. A-3 transforms the quarter space ($X, Y \geq 0$) in the complex $z = X + iY$ plane into the semi-infinite strip

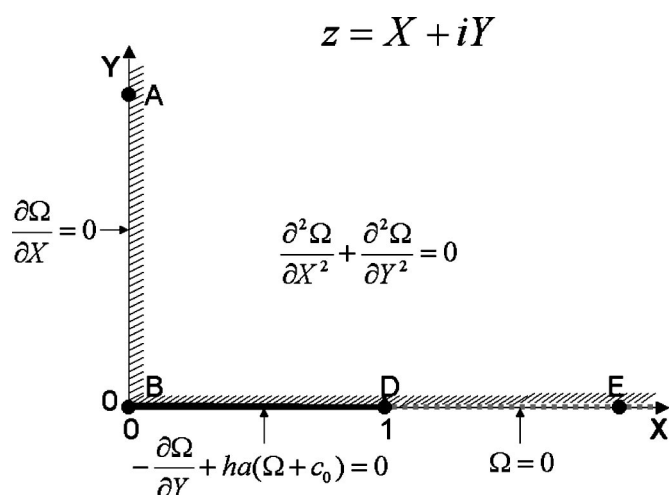


Figure 6. The quarter space “reduced” diffusion boundary value problem.

($0 \leq u \leq \pi/2, 0 \leq v < \infty$) in the $w = u + iv$ plane (Fig. 7). In this semi-infinite strip $A', B', D',$ and E' are the images, respectively, of $A, B, D,$ and E in Fig. 6; we seek a solution for $\Omega(u, v)$ to

$$\frac{\partial^2 \Omega}{\partial u^2} + \frac{\partial^2 \Omega}{\partial v^2} = 0 \quad [\text{A-6}]$$

in the semi-infinite strip with boundary conditions as shown in Fig. 7.

The solution for $\Omega(u, v)$ satisfying the boundary conditions on $u = 0$ and $u = \pi/2$ is

$$\Omega(u, v) = \sum_{n=0}^{\infty} A_n \exp^{-(2n+1)v} \cos[(2n+1)u] \quad [\text{A-7}]$$

The unknown constants A_n are determined using the remaining boundary condition on the bottom of the strip ($v = 0$) which requires that

$$\sum_{n=0}^{\infty} A_n [(2n+1) + ha] \cos[(2n+1)u] = -hac_0 \quad [\text{A-8}]$$

As is standard in problems of this type (Sturm-Liouville problems), orthogonality of the eigenfunctions $\cos[(2n+1)u]$ on the interval $[0, \pi/2]$ leads to

$$A_n = -\frac{4hac_0}{(2n+1) + ha} \times \frac{1}{(2n+1)\pi} \sin\left[(2n+1)\frac{\pi}{2}\right] \quad [\text{A-9}]$$

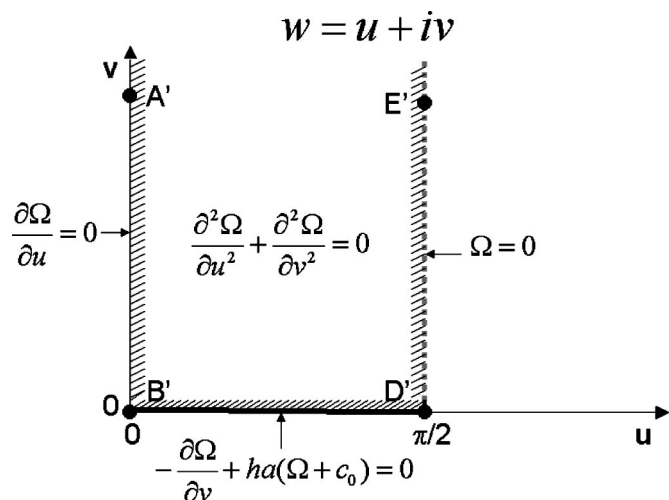


Figure 7. The semi-infinite strip diffusion problem in the $w = u + iv$ plane.

or, because $\sin[(2n+1)\pi/2] = (-1)^n$, the requisite solution for $\Omega(u, v)$ is given by Eq. A-7 with

$$A_n = -\frac{4hac_0}{(2n+1) + ha} \times \frac{1}{(2n+1)\pi} (-1)^n \quad [\text{A-10}]$$

For the present purposes, we are really interested in $\Omega(X, 0)$ when $0 \leq X \leq 1$ (the concentration along the electrode). From Eq. A-5, $Y = 0$ and $0 \leq X \leq 1$ correspond to $v = 0$ and $u = \sin^{-1} X$. Thus, the total concentration directly beneath the half-electrode is given by

$$\begin{aligned} c(X, 0) &= \Omega(X, 0) + c_0 \\ &= c_0 \left\{ 1 - \frac{4}{\pi} \sum_{n=0}^{\infty} (-1)^n \frac{ha}{(2n+1)(2n+1+ha)} \right. \\ &\quad \left. \times \cos[(2n+1)\sin^{-1} X] \right\} \quad \text{for } 0 \leq X \leq 1 \quad [\text{A-11}] \end{aligned}$$

It is easily seen that as the parameter ha tends to zero, the dimensionless concentration ratio $c(X, 0)/c_0$ tends to 1. Using the identity (Jolley²⁴)

$$\sum_{n=0}^{\infty} (-1)^n \frac{\cos[(2n+1)\theta]}{2n+1} = \frac{\pi}{4} \quad [\text{A-12}]$$

one notes that $c(X, 0)/c_0$ tends to zero for large values of ha , which is consistent with the numerical results depicted in Fig. 4 in the text.

Appendix B

We would like to use the TPB model to predict the kinetic scaling of circular Pt/Nafion microcontacts. Specifically, we are interested in how the faradaic impedance (R_f) of circular Pt/Nafion contacts scales as a function of contact size. The TPB model provides concentration profiles $[c(x, 0)]$ underneath the Pt/Nafion contacts. We convert these concentration profiles into faradaic impedance values using the following procedure.

The shape and magnitude of the concentration profiles depend only on ha . We fix h , and generate a series of concentration profiles $[c(x, 0)]_a$ for various values of a that span the range of contact size interest.

The concentration profile under the Pt/Nafion contact (for a given Pt/Nafion contact size, say $a = a_1$) is converted to a current density profile using the assumption of first-order kinetics

$$J(x, 0)|_{a=a_1} = kc(x, 0)|_{a=a_1} \quad [\text{B-1}]$$

where $J(x, 0)|_{a=a_1}$ = Current density profile for Pt/Nafion contact of half-width a_1 (A/cm^2).

This local current density profile is then applied to a circular contact geometry and integrated over that geometry to generate a total current density for the Pt/Nafion contact

$$J_{\text{tot}}|_{a=a_1} = \frac{\int_0^{a_1} 2\pi r J(r, 0)|_{a=a_1} dr}{\pi a_1^2} \quad [\text{B-2}]$$

where $J_{\text{tot}}|_{a=a_1}$ = Total current density for Pt/Nafion contact of radius a_1 (A/cm^2).

To calculate a faradaic impedance from the current density results, we assume that iR and mass-transport effects are negligible (consistent with our original model assumptions). In other words, the I-V. behavior of the Pt/Nafion contacts is dominated by Tafel kinetics over the entire potential range. In this case, R_f may be related directly to the current density evolved by the Pt/Nafion contact through the Tafel kinetics (see Ref. 23)

$$R_f = \frac{RT}{\alpha n F J_{\text{tot}}} \quad [\text{B-3}]$$

where R_f is the faradaic impedance (Ω/cm^2), α the transfer coefficient, n the number of electrons transferred, F is Faraday's constant (96,500 C/mol), R the gas constant [8.314 J/(mol-K)], and T is temperature (K). This procedure (Eq. B1-B3) are then repeated for other values of a in order to generate a curve of faradaic impedance (R_f) vs. Pt/Nafion contact size (a) over the range of interest.

Three fitting parameters are required for this procedure: D , k , and α . The following values were used to generate the model fit of the experimental data shown in Fig. 5 in the text; D_{O_2} was assumed to be $7.4 \times 10^{-7} \text{ cm}^2/\text{s}$, in reasonable agreement with previous studies as described in the text; k was assumed to be $0.0906 \text{ cm/s} = 3.47 \times 10^4 \text{ A cm/mol}$ based on the experimentally determined kinetics for the Pt/Nafion contacts detailed in Ref. 23; and α was assumed to be 0.285, also based on the experimentally determined kinetics for the Pt/Nafion contacts detailed in Ref. 23.

References

1. M. S. Wilson and S. Gottesfeld, *J. Appl. Electrochem.*, **22**, 1 (1992).
2. B. C. H. Steele, *J. Mater. Sci.*, **36**, 1053 (2001).

3. J. Mizusaki, H. Tagawa, K. Tsuneyoshi, and A. Sawata, *J. Electrochem. Soc.*, **138**, 1867 (1991).
4. M. Kleitz and F. Petitbon, *Solid State Ionics*, **92**, 65 (1996).
5. J. Fleig, *Annu. Rev. Mater. Res.*, **33**, 361 (2003).
6. A. Bieberle, L. P. Meier, and L. J. Gauckler, *J. Electrochem. Soc.*, **148**, A646 (2001).
7. V. Brichzin, J. Fleig, H. U. Habermeier, G. Cristiani, and J. Maier, *Solid State Ionics*, **152**, 499 (2002).
8. J. Fleig, *J. Power Sources*, **125**, 228 (2002).
9. R. O'Hayre and F. B. Prinz, *J. Electrochem. Soc.*, **151**, A756 (2004).
10. R. P. Iczkowski and M. B. Cutlip, *J. Electrochem. Soc.*, **127**, 1433 (1980).
11. P. D. Beattie, V. I. Basura, and S. Holdcroft, *J. Electroanal. Chem.*, **468**, 180 (1999).
12. A. Parthasarathy, S. Srinivasan, A. J. Appleby, and C. R. Martin, *J. Electrochem. Soc.*, **139**, 2856 (1992).
13. R. V. Churchill, *Complex Variables and Applications*, 2nd ed., McGraw-Hill, Inc., New York (1960).
14. A. J. Bard and L. R. Faulkner, *Electrochemical Methods*, 2nd ed., John Wiley & Sons, New York (2001).
15. A. Parthasarathy, C. R. Martin, and S. Srinivasan, *J. Electrochem. Soc.*, **138**, 916 (1991).
16. S. Mitsushima, N. Araki, N. Kamiya, and K. Ota, *J. Electrochem. Soc.*, **149**, A1370 (2002).
17. Z. Ogumi, Z. Takehara, and S. Yoshizawa, *J. Electrochem. Soc.*, **131**, 769 (1984).
18. A. Parthasarathy, S. Srinivasan, A. J. Appleby, and C. R. Martin, *J. Electrochem. Soc.*, **139**, 2530 (1992).
19. F. A. Uribe, T. E. Springer, and S. Gottesfeld, *J. Electrochem. Soc.*, **139**, 765 (1992).
20. M. A. Enayetullah, T. D. Devilbiss, and J. O. Bockris, *J. Electrochem. Soc.*, **136**, 3369 (1989).
21. S. Murkerjee, S. Srinivasan, M. P. Soriaga, and J. McBreen, *J. Phys. Chem.*, **99**, 4577 (1995).
22. J. Larminie and A. Dicks, *Fuel Cell Systems Explained*, 1st ed., John Wiley & Sons, New York (2000).
23. R. O'Hayre, G. Feng, W. D. Nix, and F. B. Prinz, *J. Appl. Phys.*, **96**, 3540 (2004).
24. L. B. W. Jolley, *Summation of Series*, 2nd rev. ed., pp. 96-97, Formula 505, Dover, NY (1961).